Novel Automated Tracking Analysis of Particles Subjected to Shear Flow: Kindlin-3 Role in B Cells

Frances Willenbrock,[†*] Daniel Zicha,[‡] Andreas Hoppe,[§] and Nancy Hogg[†*]
[†]Leukocyte Adhesion and [‡]Light Microscopy Laboratories, Cancer Research UK, London Research Institute, London, United Kingdom; and [§]Digital Imaging Research Centre, Kingston University, Kingston-upon-Thames, London, United Kingdom

ABSTRACT Shear flow assays are used to mimic the influence of physiological shear force in diverse situations such as leukocyte rolling and arrest on the vasculature, capture of nanoparticles, and bacterial adhesion. Analysis of such assays usually involves manual counting, is labor-intensive, and is subject to bias. We have developed the Leukotrack program that incorporates a novel (to our knowledge) segmentation routine capable of reliable detection of cells in phase contrast images. The program also automatically tracks rolling cells in addition to those that are more firmly attached and migrating in random directions. We demonstrate its use in the analysis of lymphocyte arrest mediated by one or more active conformations of the integrin LFA-1. Activation of LFA-1 is a multistep process that depends on several proteins including kindlin-3, the protein that is mutated in leukocyte adhesion deficiency-III patients. We find that the very first stage of LFA-1-mediated attaching is unable to proceed in the absence of kindlin-3. Our evidence indicates that kindlin-3-mediated high-affinity LFA-1 controls both the early transient integrin-dependent adhesions in addition to the final stable adhesions made under flow conditions.

INTRODUCTION

Many biological responses are influenced by the shear flow of the circulation. For example, circulating immune, tumor, and stem cells make use of adhesion receptors to undergo the transition from circulation to tissue niche (1–3). Bacteria can mimic these mechanisms (4), and it is now recognized that efficient delivery of nanoparticles in vivo has a component of shear dependence (5). However, the analysis of the shear flow assay as it is currently performed has several limitations. First, it requires prejudging and preassignment of the categories of cell behavior. Second, manual or only semiautomated tracking means that limited numbers of cells are assessed. Third, the possibility of bias is built into the assay. We here describe a robust and fully automated mechanism for tracking cells or particles under shear flow conditions that we have named the Leukotrack program. We demonstrate its use in the analysis of leukocyte attachment and migration.

Leukocyte behavior on the vascular endothelium in response to infection or injury is guided by adhesion receptors, with initial contact mediated by selectins, followed by transient attachment through integrin LFA-1 (CD11a/CD18; $\alpha L\beta_2$) that leads to slow rolling and then firm adhesion and migration. These progressive steps in leukocyte adhesion can be mimicked by the shear flow assay in which the cells contact either stimulated endothelial cells or a combination of purified integrin ligand and stimulants such as the selectins and/or chemokines (6–8). Inside-out signaling through stimulating receptors on leukocytes brings about conformational change to LFA-1 that increases its affinity for ligand intercellular adhesion molecule-1 (ICAM-1) (9–11). LFA-1 has three major conformations characterized as bent, with minimal ICAM-1-binding ability, and extended with either closed or open headpiece, the latter having the highest affinity for ICAM-1 (12,13). The extended closed form may have ICAM-1 binding activity of intermediate affinity (14). Alternatively, the intermediate affinity state may represent a mixture of closed and open headpiece integrin conformations (15).

Shear stress has a major role in generating stable adhesion. For example, for primary T lymphocytes, biological stimulants of LFA-1 activation such as chemokines, T cell receptor cross-linking, and presumably E-selectin, by themselves fail to generate sufficient high-affinity LFA-1 to rapidly promote adhesion (9,10,13,16). Instead these signaling pathways bring about an extended form of LFA-1 that is rapidly converted to the high-affinity conformation through a mechanosensory mechanism promoted by shear. Specifically, the coupling of LFA-1 to the actin cytoskeleton induces the most active integrin conformation through a subsequent allosteric switch caused by resistance to translational movement on exposure to shear stress (9,10,17,18).

The importance of the signaling leading to integrin activation is highlighted by leukocyte adhesion deficiency-III (LAD-III) patients who experience life-threatening infections as well as severe bleeding because of a failure of integrin function (19,20). The leukocytes of the LAD-III patients express integrins normally, but these integrins are inactive because of mutation in the *KINDLIN3* (*FERMT3*) gene coding for kindlin-3 that is exclusively expressed in cells of hematopoietic origin (21,22). How the kindlins contribute to

Submitted March 11, 2013, and accepted for publication June 18, 2013.

*Correspondence: nancy.hogg@cancer.org.uk or frances.willenbrock@cancer.org.uk

Editor: Rick Horwitz.

0006-3495/13/09/1110/13 $2.00

http://dx.doi.org/10.1016/j.bpj.2013.06.051

integrin activation is not fully understood. It has been proposed that the kindlins aid talin binding to the membrane proximal NPXY site of the integrin β subunit tail by binding to the membrane distil NXXY site on the β tail, thereby assisting in the induction and stabilization of the high-affinity form of integrin (19,23–26). However, the kindlins could have an indirect role. Kindlin-2 has been shown to bind migfilin, forming a complex that can uncouple the integrin negative regulator, filamin, from its binding site on the β tail, thus allowing talin to bind (25,27–29). Another possibility is that the kindlins regulate the activity of talin-bound integrin through *cis* or *trans* interactions that control clustering. Finally, they might act as scaffolds for recruiting further molecules involved in integrin function.

In the present study, we use the shear flow assay and E-selectin signaling to induce LFA-1-mediated adhesion of B cells to ligand ICAM-1, a combination that allows different stages in integrin-meditated attaching to be distinguished (8,10,30). Using the Leukotrack program to further investigate the role of kindlin-3 in LFA-1 activation, we find that kindlin-3 and talin are both required for the first slow rolling stage of B lymphocyte attaching, which is mediated by high-affinity LFA-1.

MATERIALS AND METHODS

Reagents

The α/β antagonist XVA143 (RO0281607-001) was a gift from Dr. Paul Gillespie (Roche, Nutley, NJ) (31,32). B cells were preincubated with the compound at 10 μM for 15 min prior to assay.

The following peptides were synthesized and disulphide-coupled at the N-terminus to membrane-penetrating peptides Tat or Penetratin by Nicola O'Reilly and Dhira Joshi, Protein and Peptide Chemistry (Cancer Research UK, London Research Institute, London, UK): wild-type (wt) β2 cytoplasmic tail peptide (KALIHLSDLREYRRFEKEKLKSQWNNDNPLFK SATTTVMNPKFAES), with kindlin-3 binding site altered (KALIHLSDL REYRRFEKEKLKSQWNNDNPLFKSATPTVMNPKAAES), with talin binding site altered (KALIHLSDLREYRRFEKEKLKSQWNNDNPLAK SATTTVMNPKFAES), and with both kindlin-3 and talin sites altered (23,33). All were coupled to Tat (CYGRKKRRQRRR). Migfilin peptide incorporating the filamin-binding site without (KPEKRVASSVFITLAPC) and with inactivating alterations (KPEKRVADSAFITLAPC) were coupled to penetratin peptide (RQIKIWFQNRRMKWKKC) (28,29,34). Lymphocytes were preincubated for 10 min at 37°C with peptides at 10 μM.

Leukotrack software

The developed cell-tracking algorithm was implemented as a Mathematica notebook (Wolfram Research, Champaign, IL), which calls a compiled C routine for Cell Segmentation. The software is freely available for academic research on application to Dr. Daniel Zicha (daniel.zicha@cancer.org.uk) and will run under Linux as well as Windows where installation of Cygwin (www.cygwin.com) is required. The Cygwin software is free of charge.

Cells and cell transfection

Epstein-Barr virus (EBV)-transformed B lymphoblastoid cells derived from peripheral blood mononuclear cells of Turkish LAD-III patients, their parents, and control EBV-transformed B cell lines BS or DT have all been previously reported (21). These cells were maintained in RPMI 1640 in 10% FCS (fetal calf serum).

EBV-transformed B cells (2×10^7 cells) were washed in OptiMEM+GlutaMAX (Invitrogen, Paisley, UK) and electroporated with the following reagents at 400 nM per reaction using a Gene Pulser with Capacitance Extender (Bio-Rad UK, Hemel Hempstead, UK) set at 960 μF and 300 mV: talin siRNA (Ambion, 16804: TLN-1 ID:5552), filamin A, and B siRNAs (Filamin A: Dharmacon ON_TARGET plus SMARTpool L-012579-00. Filamin B: Invitrogen Stealth HSS103736) or negative control siRNA. Individual knockdowns were evaluated by blotting using either antitalin mAb 8d4 (Sigma T3287) or rabbit antihuman pAbs specific for kindin-3 (21), filamin A (Millipore AB9276), or filamin B, a gift from Dr. Dave Calderwood, Yale University.

Preparation of flow chamber

ibiTreat μ-slide VI channels (ibidi, Martinsried, Germany) were initially coated with protein A (0.5 mg/ml in phosphate buffered saline (PBS); Sigma-Aldrich Ltd., Gillingham, Kent, United Kingdom) overnight at 4°C. The following day, unoccupied sites on the channels were blocked by incubation with 5% BSA (bovine serum albumin) in PBS for 30 min at room temperature and this was followed by E-selectin-Fc (0.5 μg/ml, R&D Systems Europe, Abingdon, UK) and ICAM-1-Fc (20 μg/ml; as prepared previously (35)) in a total volume of 40 μl in 0.2% BSA in 0.1M citrate pH 6 for 20 min at room temperature. The chambers were washed with 20 mM HEPES in HBSS before use. ICAM-1-Fc and E-selectin-Fc were demonstrated to be uniformly distributed by analyzing binding of the proteins labeled with Alexa-Fluor 488 using a Zeiss LSM510 Axioplan2 Inverted confocal microscope with a 63× NA1.4 Plan-Apochromat oil immersion objective lens. The relationship between fluorescence and concentration of labeled ICAM-1-Fc was shown to be linear up to concentrations of 50 μg/ml in a volume of 40 µl, demonstrating that protein A binding sites were not saturated at the concentrations used in the assay. We could therefore assume complete binding of both E-selectin-Fc and ICAM-1-Fc in our assay and calculate site densities for ICAM-1-Fc and E-selectin-Fc of ~7500 and 600 sites μm^{-2}, respectively.

Shear flow assays

The shear flow assay was performed on E-selectin-Fc with and without ICAM-1-Fc at 37°C in 20 mM HEPES in HBSS (pH 7). Flow conditions of 2 dyn cm^{-2} were used unless otherwise stated and the cells pumped through the flow chamber at a cell density of up to 5×10^5 cells/ml in 1% human serum in 20 mM HEPES/HBSS using an automated syringe pump (KDS Model 200, Linton Instrumentation, Norfolk, UK) as previously reported (35). The adhesion characteristics of B cells were recorded using a Nikon Diaphot 300 microscope with a Sony XCD-X700 camera using a 10× lens and AQM^{2001} Kinetic Acquisition Manager software (Kinetic Imaging, Bromborough, UK). The flow system was run for 3 min before recording was started and then images were captured every second for 15 min. Videos from three separate areas of each flow chamber experiment were recorded.

LFA-1 activation mAb assays

Assays were performed under shear flow at 2 dyn cm^{-2} using channels that had been coated with protein G (0.5 mg/ml in PBS) followed by 0.5 μg/ml E-selectin and 20 μg/ml of pan-LFA-1 mAb TS1/18 (36), β2 integrin extension mAb KIM127 (37), or β2 integrin high-affinity epitope mAb 24 (38). Separate sets of channels were coated with mAb only and were run at 0.2 dyn cm^{-2} to give rates of B cell displacement that mimicked rolling in the presence of E-selectin. The assay was run for 15 min, and then the

channel was washed with 20 mM HEPES in HBSS for 5 min at 2 dyn cm^{-2}. The number of cells that remained attached were counted along the length of the channel.

Statistics

To determine the average rate of cell movement in the flow assays, we determined the mean of the rates of the total population of cells in each run. Assays were calibrated to allow for any variation in coating by using E-selectin only. Results were analyzed to give the mean ± standard deviation of the mean rate of movement for each run and statistical significance was determined by one-way analysis of variance with Bonferroni multiple comparison test. All analyses were performed using GraphPad Prism software. Significant differences are as indicated: $*p < 0.05$, $**p < 0.01$, $***p < 0.001$. The deviation in rolling velocity was determined as previously described (39).

RESULTS

Leukotrack automated tracking program

When lymphocytes flow over a substrate of E-selectin and ICAM-1 under shear flow conditions, they roll in the direction of flow and may adhere both transiently and for longer periods followed by migration in any direction. The challenges in automatically tracking such varying behavior in a flow assay are twofold in that there is heterogeneity in both the appearance and the behavior of the cells. Although it is possible to circumvent these problems by using conditions that favor either attachment or rolling only, we wished to be able to analyze all types of cell behavior under comparable conditions. Thus, the aim of the development of the Leukotrack program was to achieve high reliability of automatic detection and tracking of every cell in the flow assays.

The main challenges come from the phase contrast imaging of the cells. Not only do the cells usually have dark centers surrounded by bright halo, but also when they attach to the substrate, their shape and appearance change significantly. An additional complication arises from the fact that fast-moving floating cells, which do not show any attaching behavior, produce undesirable streaks in the images. Therefore, we decided to introduce a *spatial* multiscale approach that deals robustly with the changing appearance of cells while rejecting streaks and small debris. Subsequently, we allowed multiple assignments for individual cells that are eventually resolved in the tracking phase using *temporal* continuity of individual cells resulting in a single track for each cell.

Cell segmentation

In the first step, we applied a 3×3 high-pass Prewitt filter to the phase contrast images enhancing cellular regions as well as other features in the image, such as debris and streaks (Fig. 1 *A*). To distinguish cells from debris and streaks, we adopted an image segmentation approach on the basis of scale-space image analysis (40). In scale-space analysis, images can be viewed as being composed of features at different scales s. Therefore, we produced images of reducing scales $I(x,y,s)$ by iterative convolution with Gaussian kernel (Fig. 1, *B* and *C*) where features blur with increasing scale and eventually diffuse into the background. Cellular regions can be identified by high levels of cumulative diffusion rate.

The diffusion rate for each pixel position at each scale s can be calculated as the intensity differential between images at subsequent scales $I(x,y,s) - I(x,y,s+1)$ and areas with higher contrast will thus express higher diffusion rates. The background areas of low contrast will result in low diffusion rates. Small debris only initially express high diffusion rates and then quickly diffuse into the background, whereas streaks produce low diffusion rates throughout (Fig. 1 *F*). In both cases, the cumulative diffusion rate is low. Cellular regions, however, produce higher positive diffusion rates over more scales, thus achieving high cumulative rates. To distinguish the two situations, we combined and thresholded the weighted (multiplied by s) positive diffusion rates over a number of scales m to form a segmentation image I_{segm} as shown in Eq. 1:

$$I_{segm} = \frac{\sum_{s=1}^{m-1} s\left\{\begin{array}{cc} I(x,y,s) - I(x,y,s+1) & \text{if } I(x,y,s) - I(x,y,s+1) > 0 \\ 0 & \text{otherwise} \end{array}\right\}}{\sum_{S=1}^{m-1} S} > T, \quad (1)$$

where T is user defined threshold, m is the number of iterative scales, and I_{segm} is the segmented binary image containing cellular regions. Cellular regions are subsequently identified and labeled using 4-connectivity at the pixel level (Fig. 1 *D*), and centroid positions of the cellular regions (Fig. 1 *E*) are calculated and exported for the tracking procedure.

Cell tracking

Commercially available tracking methods match cells in consecutive frames on the basis of distance alone and are not reliable in shear flow assays because the distance between a rolling and static cell in consecutive frames is often less than that traveled by the rolling cell, leading to incorrect joining tracks of rolling and migrating cells (Fig. 2 *A*). Our approach was to exploit the different

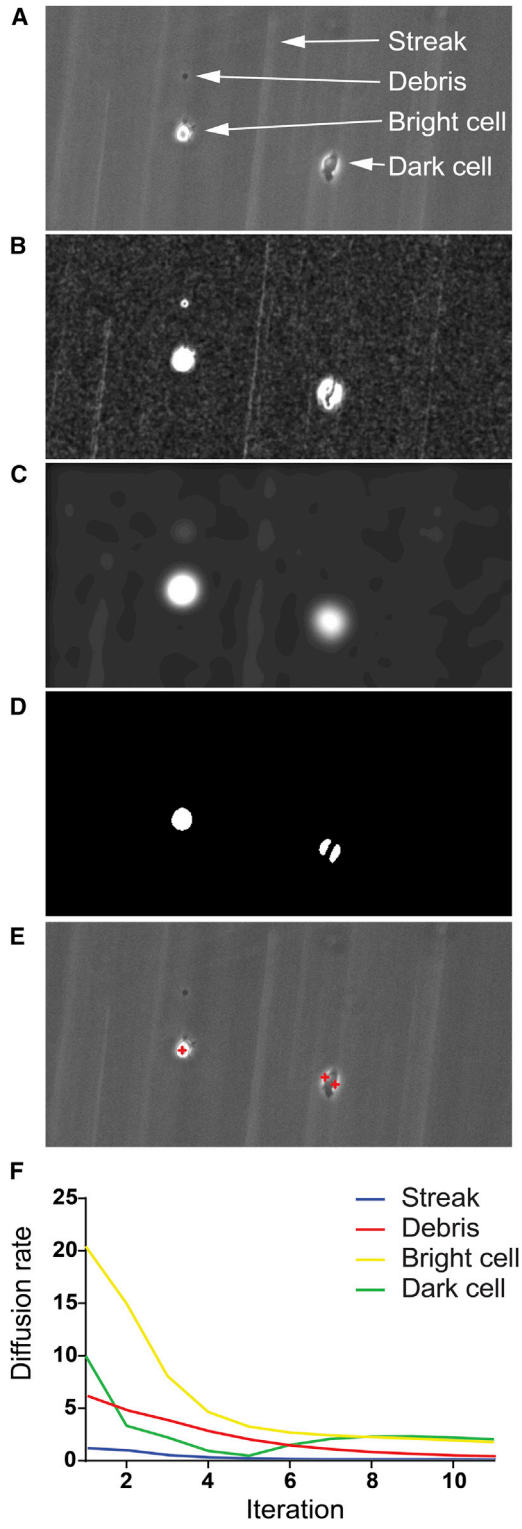

FIGURE 1 Illustration of the image segmentation process. (*A*) Phase contrast image with highlighted streak, debris, bright cells, and a dark cell. (*B*) Image after application of high-pass filter and the first convolution iteration. Streaks, debris, and cells are enhanced. (*C*) Image after the ninth convolution iteration. Debris and streaks express lower intensities, whereas cells are still clearly visible. (*D*) Segmented image of cumulative diffusion rate after a threshold has been applied (Eq. 1). The dark cell is represented by two different fragments. This was allowed to happen as moving fragments would later be resolved in the tracking process. (*E*) Centers of identified cells and fragments of cells are marked with *red crosses* and overlaid with the original phase contrast image. The coordinates of the tracks feed into the tracking process. (*F*) Plot of diffusion rates for the debris, the streak, the bright cell, and the dark cell. The diffusion rate is expressed as a function of iterations. Streaks express a low decreasing diffusion rate. Debris expresses initially a higher diffusion rate that decreases and approaches that of streaks after 10 iterations. Bright cells express a high diffusion rate that decreases over time but remains above that of debris and streaks after 10 iterations. Dark cells with low contrast only initially express a higher diffusion rate that quickly decreases and then increases again. The weighted cumulative sum of the diffusion rates provides a robust means to distinguish between cells with low and high contrast from debris and streaks.

predicted trajectories of arrested/migrating cells and rolling cells. Thus, the path of a randomly migrating cell lies within a circular probability distribution, with the center of the circle being the original position of the cell. The path of a rolling cell, however, is distorted by the force of the flow so that this circular distribution transforms to an elliptical one, with its major axis in the direction of the flow and length of the semimajor axis equivalent to the average distance traveled by the rolling cell.

Cells that are attached throughout the assay are initially removed by performing a preliminary tracking process based on the shortest distance between positions of cells in consecutive frames with displacement size set at less than 17 μm. An attached cell is defined as one in which the average displacement between frames is lower than 0.8 μm for at least 15 frames. Each of these parameters can be adjusted by the user.

The remaining cells consist of fast- and slow-rolling cells and also cells that initially roll and then attach and migrate. Displacements of rolling cells are greater than those of attached cells; therefore, the use of a tracking procedure that is based on the nearest neighbor principle results in tracks of rolling cells incorrectly joining with those of attached cells. Therefore, we chose to exploit the difference in trajectories of rolling cells, which move primarily in the direction of flow, compared with arrested and migrating cells, which migrate in random directions (Fig. 2 *A*). Thus, in contrast to the displacements of migrating cells, which fit a 2D circular Gaussian distribution, displacements of rolling cells are biased in the direction of the flow and fall within a probability distribution defined by a 2D elliptical Gaussian distribution with major axis aligned with the direction of flow (Eq. 2 and Fig. 2, *B* and *C*):

$$f(x,y) = Ae^{-\left(a(x-x_0)^2+2b(x-x_0)(y-y_0)+c(y-y_0)^2\right)}, \qquad (2)$$

in which

$$a = \frac{\cos^2\theta}{2\sigma_x^2} + \frac{\sin^2\theta}{2\sigma_y^2},$$

$$b = \frac{-\sin 2\theta}{4\sigma_x^2} + \frac{\sin 2\theta}{4\sigma_y^2},$$

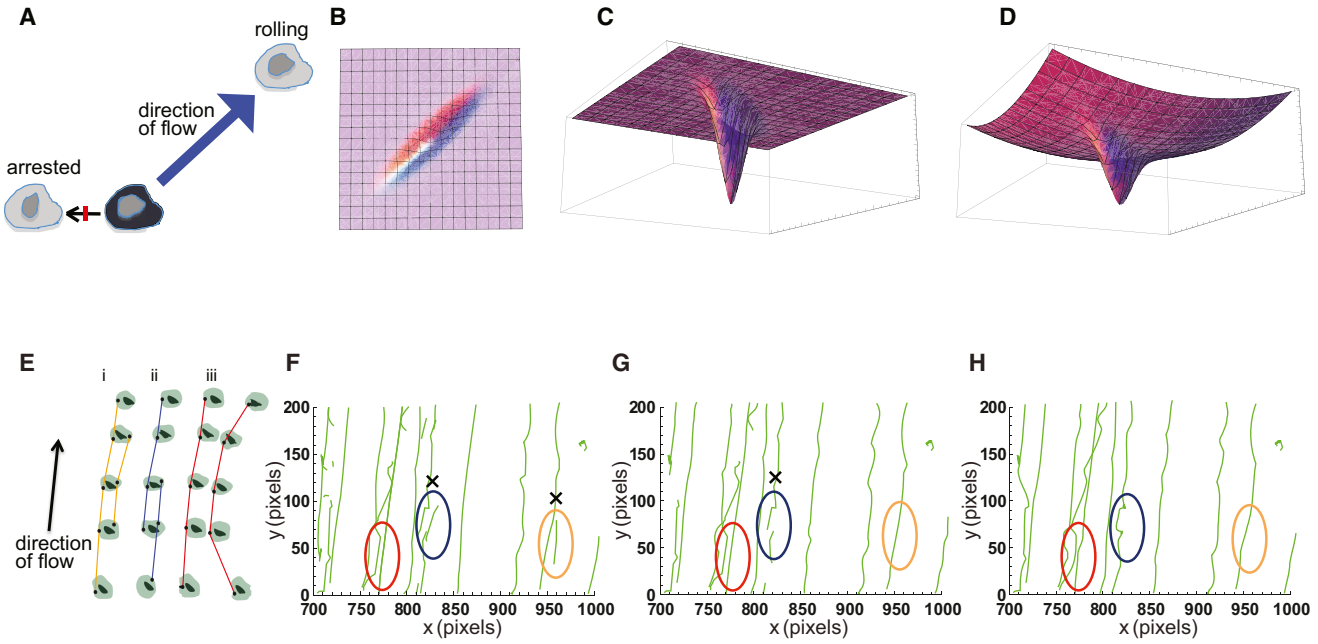

FIGURE 2 Elliptical distribution of EBV-transformed B cells rolling under shear flow. (*A*) Schematic demonstrating failure of tracking using nearest neighbor principle. The light cells represent possible positions of the dark cell in the subsequent frame. A rolling cell travels farther than an arrested cell but would be incorrectly tracked to the position of the labeled arrested cell. (*B*) and (*C*) Graphical representation of the 2D Gaussian described by Eq. 2 depicted from directly above (*B*) and below and at an angle (*C*). (*D*) Graphical representation of the 2D Gaussian described by Eq. 4 showing the impact of combining elliptical and circular Gaussian distributions. (*E–H*) Examples of parallel tracks that can arise from multiple cell assignments and their corrections. (*E*) Graphic depiction of parallel tracks that can arise from multiple cell assignments that are corrected in a small part of a movie in which the individual cell tracks (*green*) move in the direction of flow. (*F–H*) Examples are orange (*i*) and blue (*ii*) ovals, overlapping tracks that are incorrectly assigned, then corrected; red oval (*iii*), two cells moving in parallel where the tracks are correctly assigned.

$$c = \frac{\cos^2\theta}{2\sigma_y^2} + \frac{\sin^2\theta}{2\sigma_x^2},$$

where A is the amplitude, x_0 and y_0 represent the center, σ_x and σ_y are measures of the spread of the distribution, and θ is the flow direction.

Both types of cell behavior can be tracked simultaneously by combining the normalized elliptical Gaussian distribution (Eq. 3) with the circular Gaussian to produce the penalty function $p(x,y)$ (Eq. 4 and Fig. 2 *D*):

$$f'(x,y) = A' e^{-\left(a(x-x_0)^2 + 2b(x-x_0)(y-y_0) + c(y-y_0)^2\right)}, \qquad (3)$$

in which A' is the normalized amplitude:

$$p(x,y) = (x-x_0)^2 + (y-y_0)^2 - k\left(x_0^2 + y_0^2\right)\left(f'(x,y) - 1\right), \qquad (4)$$

where k is a constant determining the relative contribution of the elliptical Gaussian. This value is empirically determined and can be entered as an advanced parameter. The default value is 8, which we have found to be optimal for our experimental conditions. For fitting to Eq. 4 to reach a global minimum reliably, we found it necessary initially to seed values of θ, σ_x, and σ_y. To obtain these values, we initially tracked cells using the nearest neighbor criteria, which resulted in several incorrect assignments, but allowed the elliptical distribution of displacements to be identified and approximate parameters to be obtained.

The application of the penalty function in Eq. 4 results in a process in which decisions follow the inverted 2D elliptical Gaussian function around its trough, whereas the nearest neighbor principle dominates away from the trough. Thus, effectively, the procedure initially assumes the cell is rolling and searches along the path of flow in the following frame for its next position. If no cell is identified in this limited area, the nearest neighbor principle is used because the elliptical Gaussian function becomes flat once away from the trough and stops producing useful information for tracking. In effect, this process checks for and tracks arrested/migrating cells. If no cell was detected with a penalty function lower than a specified limit in the following frame, we concluded that the cell had detached and the track is terminated.

After the fitting process, the two data sets for the attached cells and rolling cells are combined and tracks of cells that show both behaviors are joined by a further tracking process using Eq. 4. The final step is to remove additional tracks resulting from individual cells being detected as multiple separate objects in the segmentation process, and this is performed using an algorithm that keeps only one object per

cell (Fig. 2, *E–H*). This algorithm tests each object track for coincidence with other object tracks running in parallel within a specified distance representing the maximum size of the cell, a parameter that can be entered. Tracks are assessed based on two criteria: (a) if there is another longer track along the full length of the tested track (Fig. 2 *E(i)* and orange oval), then it is rejected; and (b) if there is only a partial overlap (Fig. 2 *E(ii)* and blue oval), the algorithm follows both tracks along their length to assess whether they are diverging. Divergence (Fig. 2 *E(iii)* and red oval) indicates the real collision of two cells and both tracks are retained. However, if tracks are parallel throughout their length, then this indicates multiple assignment and one is terminated. Finally, because this procedure gives new track ends, there is a further round of joining of tracks. Fig. 2, *F–H*, shows the result of this algorithm on tracks of B cells interacting with E-selectin and ICAM-1 under flow conditions.

Accuracy of the tracking method was assessed by observing 100 movies (averaging 106 cells per movie) with the tracks overlaid as dragontails under a number of conditions of cell density and substrate concentration (see Movie S1 in Supporting Material). The only condition that was found to reduce the accuracy was having an initial cell density of $> 5 \times 10^6$ cells/ml and when a large number of cells became attached (> 50 in a frame of 800 μm by 800 μm at $\times 10$ resolution). Under these circumstances, rolling cells collided frequently with the attached cells, resulting in breaking of tracks. We therefore chose to use a lower cell density with a longer assay time to avoid cell collisions. Under such conditions, the following statistics were observed: 96.9% of the total cells were correctly detected, correction of parallel tracks was successful for 94.6% of the rolling cells and for 78.7% of migrating cells, and 96.2% of tracks were correctly assigned along their entire length.

Implementation

Data from assays should be stored as individual .tiff files in separate folders for each movie. Sets of movies can be loaded and processed without the need for further manual input once parameters have been set. Basic settings allow the user to enter (a) calibration factors for pixel to μm conversion and (b) the lapse interval. The program displays the tracks formed after each stage of the procedure along with an option of using dragontails of the tracks on the movie so its accuracy can be checked. There are also advanced level settings, which can be accessed to further optimize cell segmentation and tracking. Once parameters have been established, they can be used to analyze batches of movies.

The tracked data are stored in a single file containing the cell index, frame numbers, and the x and y coordinates of each cell. This file is in a format that can be imported into Microsoft Excel for analysis if required.

Quantification of leukocyte behavior in the automated shear flow assay

The rate at which each cell moves throughout the assay was obtained from the median of the total displacement distances for each track. In the presence of E-selectin alone, leukocyte behavior is defined as "fast rolling," whereas contact with both E-selectin and LFA-1 ligand ICAM-1 results first in slower rolling and then cell arrest (Fig. 3 *A*). Definitions of these two ICAM-1-dependent stages are based on the time period of leukocyte attachment and have been variably assigned in the literature (Table 1), so it was important to be able to use the data in an unbiased way to establish the range of values defining cell behavior in our assay.

Alternatively, the necessity for definition of types of behavior could be removed by analyzing the average rolling rate of the total cell population in the assay compared with control B cells rolling on E-selectin alone or on E-selectin with ICAM-1. When we chose to categorize cell behaviors, all tracks with rates of ≤ 1.1 μm s^{-1} were considered to be arrested or migrating cells. This number was obtained by recording rates of migrating cells in several movies and noting the maximum value. Slow-rolling cells were then defined as those cells with a rolling rate less than on E-selectin alone but greater than 1.1 μm s^{-1}.

The rolling and migration characteristics of LAD-III B cells

We used the shear flow assay to investigate the rolling and adhering characteristics of EBV-transformed B lymphoblasts (B cells) that either expressed kindlin-3 or were from LAD-III patients that lacked this protein (21). We used a combination of E-selectin and ICAM-1 that stimulated neutrophil rolling (7,39,41,42) and that we previously found to stimulate T lymphocyte rolling and adhesion (35). Both fast- and slow-rolling speeds and arrest of control B cells and the B cells from the heterozygous unaffected parent of a LAD-III patient were similar (Fig. 3 *A*). For the LAD-III B cells, however, the absence of kindlin-3 prevented both B cell slow rolling and arrest and resembled rolling on E-selectin alone (Fig. 3 *A*). Similar results were obtained using two different sets of LAD-III patient/parent B cells (Fig. 3 *B*). Depiction of these data as the average rolling rate of the total population shows the patient cells not to be significantly different from those on E-selectin alone, confirming a total lack of LFA-1-mediated attaching (Fig. 3 *C*). We next plotted the deviation in rolling velocity on E-selectin and E-selectin/ICAM-1 to ascertain the variation in rolling by the different cell types (39). We observed the deviation in rolling on ICAM-1 to be substantially greater than rolling on E-selectin alone (Fig. 3 *D*). Another important issue to establish was whether the B cell rolling stage preceded or followed attaching on ICAM-1 as this would have implications in terms of any role played by

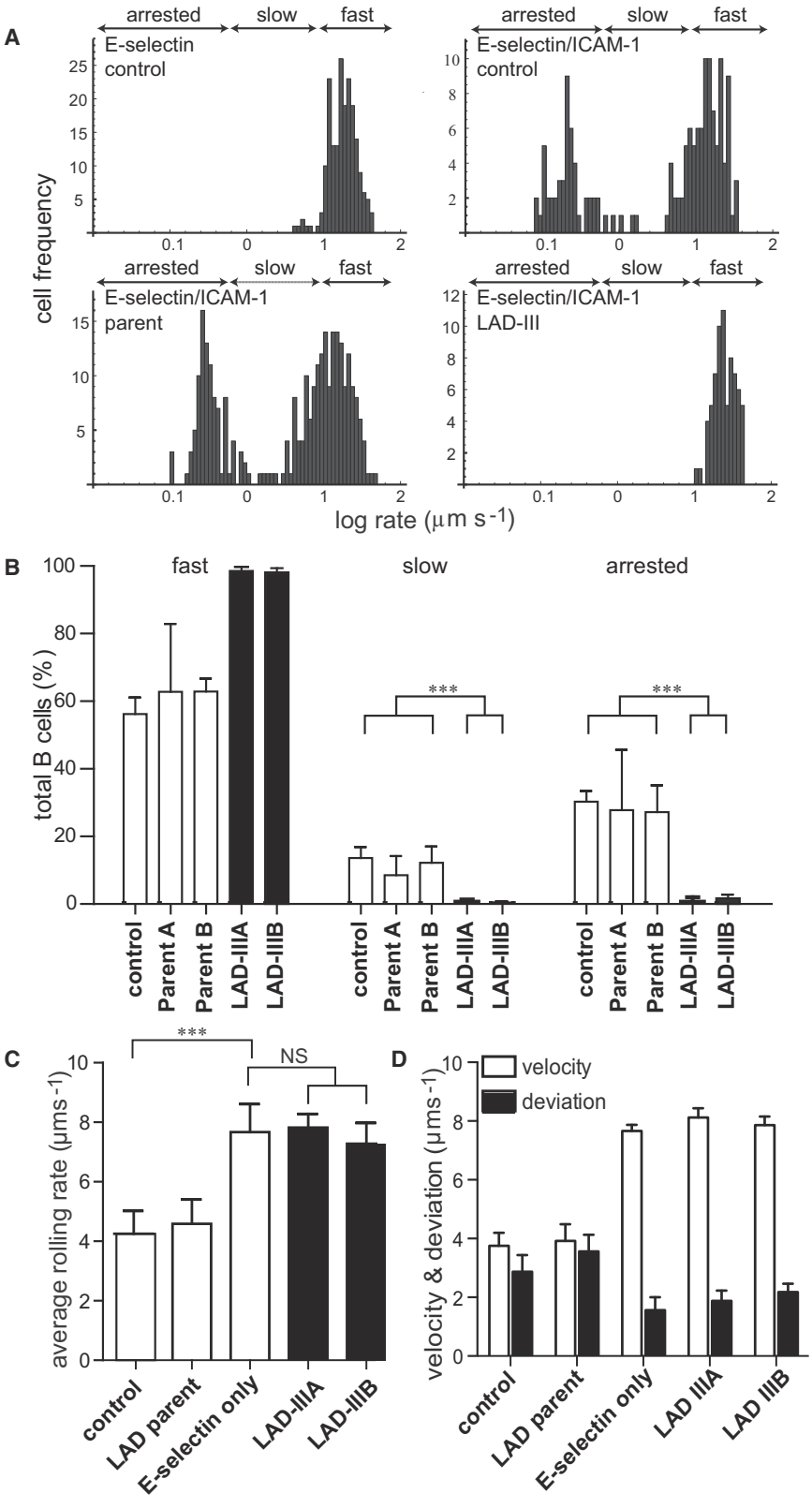

FIGURE 3 Use of the Leukotrack program to show the behavior of LAD-III, parent, and control B lymphoblasts in a shear flow assay. (*A*) Representative data showing adhesive activity of a control EBV-transformed B cell line on E-selectin alone or E-selectin/ICAM-1 compared with parent and LAD-III patient B cells on E-selectin/ICAM-1; $n = 100$–300 cells per condition. (*B*) Histogram showing rates of rolling on E-selectin/ICAM-1: control B cell line, two matching parent and LAD-III patient B cell lines. Data sets were analyzed using one-way analysis of variance for each behavior ($n = 14$ movies for control and parent, data are shown as mean ± *SEM*; $n = 8$ movies for patient A, $n = 8$ movies for patient B, $^{***}p < 0.0001$). (*C*) Summary of data in (*B*) depicted as the average rate of rolling of the total cell population for each group of cells. The E-selectin data were obtained using control B cells flowing over E-selectin only. (*D*) The standard deviations of the mean are plotted alongside the mean rolling velocity for control, parent, and patient cells rolling on E-selectin and ICAM-1 and for control cells rolling on E-selectin only. Data represent mean ± *SEM* for 200 cells in four separate assays.

E-selectin. We found that the majority of B cells rolled first and then attached (8.5%) rather than the reverse (1.8%) (Fig. S1).

Thus, kindlin-3 appears to have an essential role at the earliest stage of LFA-1 binding to ICAM-1 when the lymphocyte rolling quickly on E-selectin is slowed down

TABLE 1 Parameters used to define the behavior of leukocytes in the shear flow assay

ANALYSIS OF ARRESTS ON ICAM-1:		
Transient arrest (s)	Firm arrest (s)	Reference
<2	>3	(49)
>1	>10	(56)
0.5–10	>10	(44)
<5	>20	(57)
n/a	>30	(39)
n/a	>30	(58)
ANALYSIS OF ROLLING VELOCITY ON ICAM-1:		
−ICAM-1	+ICAM-1	
2 μm/s	1 μm/s	(59)
6 μm/s	2 μm/s	(42)

In the literature, widely varying times are used to define transient attaching and firm arrest times as well as the analysis of the effect that attaching to ICAM-1 has on the velocity of flow. These choices are made by the investigator and the data for the assays are subsequently assigned to a particular category.

by the formation of short-lived attachments on ICAM-1 that eventually lead to more stable adhesions and migration. The greater deviation in the ICAM-1 slow-rolling rate might reflect differential activation of LFA-1 by E-selectin signaling in the B cells.

A role for both kindlin-3 and talin in B cell slow rolling

LFA-1 extension is a necessary component of both T cell and neutrophil transient attachment and slow rolling (43–46). This change in conformation comes about as a result of talin binding that disrupts the salt bridge between α and β subunits of the integrin heterodimers, allowing the bent conformation to extend (47). Therefore, we next investigated whether the expression of talin was altered in LAD-III B cells and by inference whether it was sufficient for slow rolling. Western blotting revealed equivalent amounts of the talin, but complete absence of kindlin-3 in LAD-III patient B cells compared with control B cells (Fig. 4 *A*). Thus, normal levels of talin were not altered by the absence of kindlin-3, but were insufficient for supporting transient B cell adhesions.

To further investigate the relationship between kindlin-3 and talin in slow rolling, we talin siRNA treated normal EBV-transformed B cells, reducing the levels of talin by 74.5 ± 4.8% compared with control siRNA-treated B cells ($n = 7$) (Fig. 4 *B*). Under these levels of talin reduction, kindlin-3 levels were unaffected. The average rate of rolling of talin-depleted B cells on E-selectin and ICAM-1 was similar to untreated control B cells rolling on E-selectin alone and significantly greater than B cells treated with control siRNA (Fig. 4 *C*). Alternatively, when the data were displayed as cell frequency versus velocity, a 30% decrease in slow-rolling and arrested B cells treated with talin siRNA was revealed compared with B cells treated with control

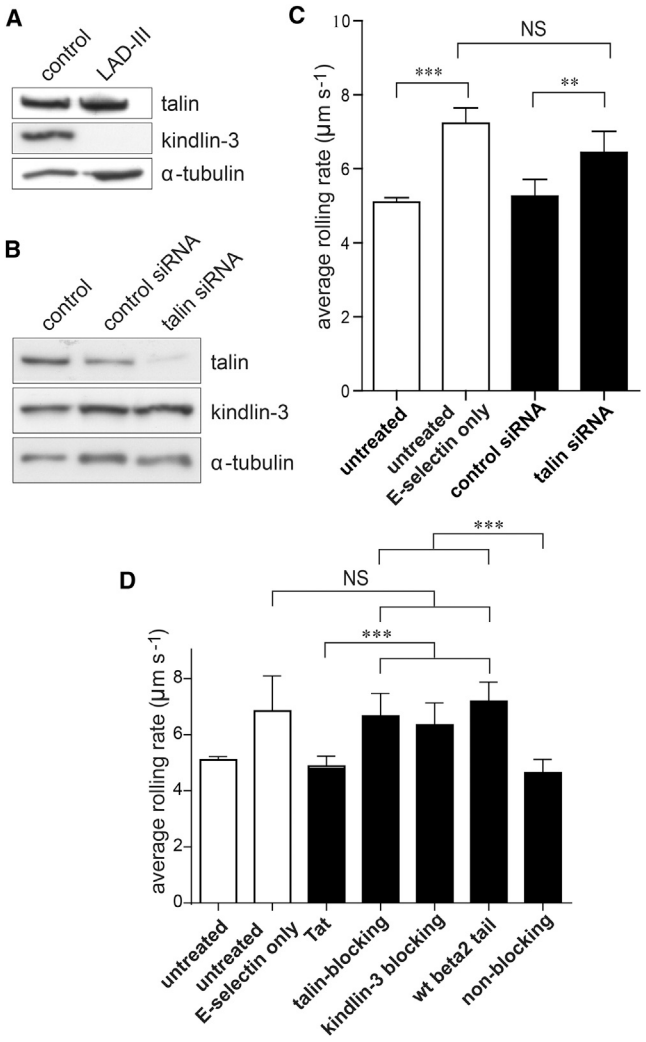

FIGURE 4 The effect on rolling rates of blocking talin and kindlin-3 function in B cells. (*A*) Western blot of control and LAD-III patient B cells showing expression levels of talin and kindlin-3; α-tubulin represents the sample loading control. (*B*) Western blot showing expression level of talin reduced to (25.5 ± 4.8%, $n = 7$) and kindlin-3 in control B cells transfected with either control siRNA or talin siRNA; α-tubulin represents the sample loading control. (*C*) Rates of rolling of either untransfected B cells rolling on E-selectin/ICAM-1 and E-selectin alone (untreated, *white bars*) compared with B cells transfected with either control or talin siRNAs on E-selectin/ICAM-1 (transfected, *black bars*); $n = 6$ independent experiments. Data are shown as mean ± *SEM*; ***$p < 0.001$; **,$p < 0.01$. (*D*) Rates of rolling of either untreated B cells on E-selectin/ICAM-1 or E-selectin alone (untreated, *white bars*) compared with B cells on E-selectin/ICAM-1 treated with Tat peptide (Tat) or LFA-1 β2 cytoplasmic tail peptides: wild-type sequence (wt β2 tail), talin-binding site modified (kindlin-3 blocking), kindlin-3-binding site modified (talin blocking), both talin and kindlin-3 sites modified (nonblocking) (*black bars*); from $n = 5$ independent experiments. Data are shown as mean ± *SEM*; ***$p < 0.001$.

siRNA (Fig. S2). These data indicate that LFA-1 activation had been impaired by talin knockdown, confirming that talin was required for slow rolling.

To compare the relative contributions of kindlin-3 and talin, we treated B cells with Tat-coupled β2 subunit tail

peptides that were either of normal sequence (wt β2 tail) or with altered kindlin-3 NPKF (talin-blocking) or talin NPLF (kindlin-3-blocking) binding sites or with both sites modified (nonblocking). The wt β2 tail peptide with unaltered kindlin-3 and talin binding sites acted in a dominant interfering manner, causing diminished slow rolling in treated B cells compared with untreated B cells or B cells expressing the Tat peptide alone and resembled B cells rolling on E-selectin alone (Fig. 4 *D*). The B cells treated with β2 peptides modified either at the talin or kindlin-3 sites also had a mean flow rate resembling that on E-selectin alone, indicating that each caused a blocking effect resulting in failure to perform LFA-1-mediated slow rolling (Fig. 4 *D*). In contrast, the peptide with both kindlin-3 and talin sites modified failed to alter the slower rolling rate. Thus, the peptide experiments further support essential roles for both kindlin-3 and talin in slow rolling. The results also are in keeping with there being direct competition between the peptides and the LFA-1 β2 cytoplasmic tail for binding kindlin-3 and talin, indicating that the β2 subunit is the point of contact for both proteins.

Lack of evidence for an indirect kindlin-3 role in LFA-1 function

To further address the question of whether kindlin-3 supports slow rolling by direct binding to LFA-1 or through interactions that indirectly alter the integrin's function, we investigated the possible roles of migfilin and filamin in LFA-1 activation, both of which have been implicated in kindlin-2 function (25,27–29).

When B cells were treated with filamin A and B siRNAs either separately or together, there was significant reduction in expression of both proteins by 82.4% and 74.7%, respectively, but no alteration in the velocity of rolling (Fig. 5 *A,B*). In addition, a similar lack of impact on slow rolling was observed when B cells were treated with migfilin peptides with or without an altered filamin binding site (Fig. 5 *C*) (28,29). Thus, an indirect role for kindlin-3 involving migfilin and filamin does not appear to be part of B cell attaching events, at least at this stage of the adhesion cascade of reactions.

Slow rolling and high-affinity LFA-1

The requirement for both kindlin-3 and talin in slow rolling of B cells implicates high-affinity LFA-1 in this phase of ICAM-1 attaching. The α/β antagonist XVA143 allows integrin extension, but binds to the βI domain at its point of contact with the I domain of the α subunit, thus interfering with full opening of the headpiece and preventing the open high-affinity LFA-1 conformation (31,32). Incubation of B cells with XVA143 results in an average rolling rate comparable to that of E-selectin alone, indicating that LFA-1 extension is not sufficient for slow rolling and implying a need for LFA-1 in the high-affinity conformation for all ICAM-1 attaching events under shear flow conditions (Fig. 6 *A*).

To more directly assess the conformation of the LFA-1 involved in slow rolling, we quantified the binding of control and LAD-III patient B cells to immobilized mAb

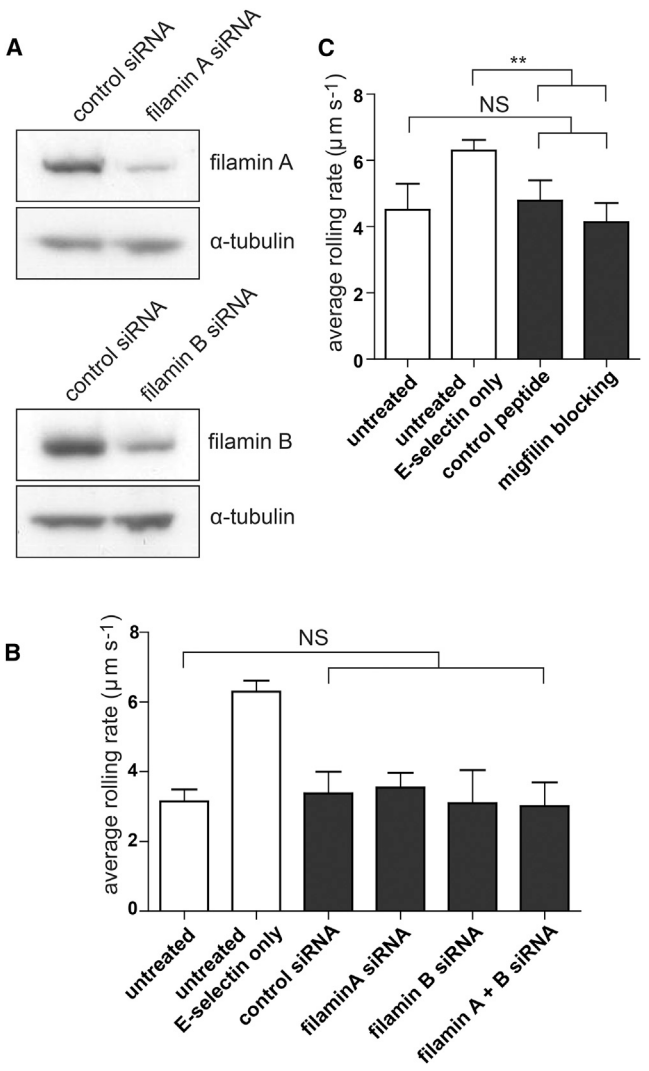

FIGURE 5 The effect of blocking filamin and migfilin function on rolling rates of B cells on E-selectin/ICAM-1. (*A*) Western blot showing expression level of filamins A (reduced to 17.6% ± 3.6, $n = 3$) and B (reduced to 25.3 ± 2.5%) in control B cells treated with either control siRNA or filamin siRNA; α-tubulin represent the sample loading control; $n = 2$. (*B*) Rates of rolling of untreated B cells rolling on E-selectin/ICAM-1 (control) or E-selectin alone (E-selectin) (*white bars*) compared with B cells on E-selectin/ICAM-1 treated with either control siRNA or filamins A and B siRNAs either individually or together (*black bars*) from $n = 3$ independent experiments. Data are shown as mean ± *SEM*; NS = not significant. (*C*) Rates of rolling of untreated B cells rolling on E-selectin/ICAM-1 or E-selectin alone (untreated, *white bars*) compared with B cells on E-selectin/ICAM-1 treated with control migfilin peptide with modified filamin binding site (control) or with an intact filamin-binding site (migfilin blocking) (*black bars*) from $n = 3$ independent experiments. Data are shown as mean ± *SEM*; NS = not significant.

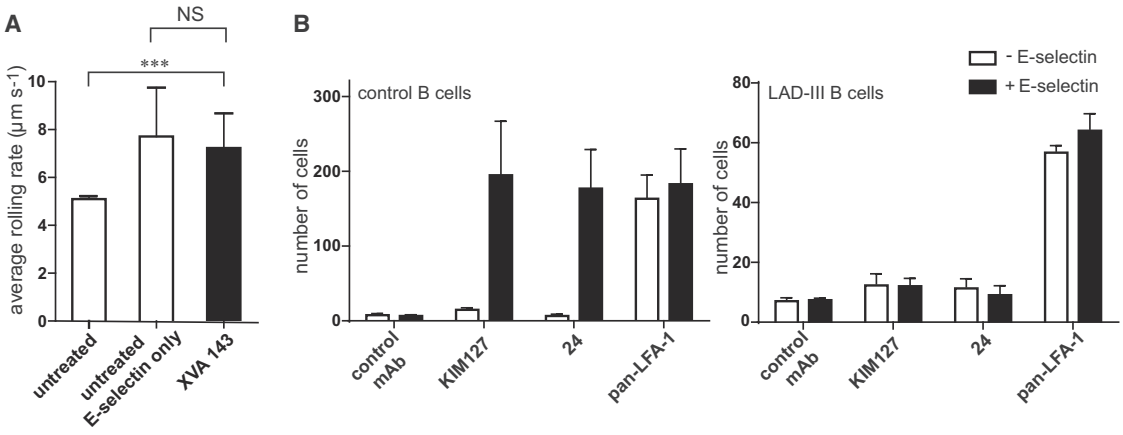

FIGURE 6 The activation state of LFA-1 after B cell stimulation through E-selectin binding. (*A*) Rates of rolling of untreated B cells on E-selectin/ICAM-1 (control) or E-selectin alone (E-selectin) (*white bars*) compared with B cells on E-selectin/ICAM-1 treated with the inhibitor XVA143 (*black bar*). (*B*) Numbers of control and LAD-III B cells attached by pan-LFA-1 mAb, $\beta 2$ extension mAb KIM127, activation mAb 24, or isotype control mAbs following exposure (*black bars*) or not (*white bars*) to E-selectin; $n = 3$ independent experiments. Data are shown as mean $\pm$ *SEM*.

KIM127, which detects extended LFA-1, and mAb 24, which binds the open high-affinity conformation of LFA-1 following exposure to E-selectin (37,38). To compare the B cell behavior in the presence of E-selectin versus its absence, it was necessary to match the slowing effect of E-selectin with equivalent cell displacement in its absence via a lower flow rate. The result was that there was no attaching to mAbs KIM127 or 24 in the absence of E-selectin, but the B cells did attach to pan-LFA-1 mAb (Fig. 6 *B*). In contrast, rolling of B cells over E-selectin caused attaching not only to the pan-LFA-1 mAb but also to the LFA-1 activation mAbs. In no circumstance did the B cells attach to isotype control mAb. In addition, the LAD-III patient cells showed no E-selectin-mediated LFA-1 activation in terms of binding to mAbs KIM127 or 24 (Fig. 6 *B*). These data provide further evidence that B cell slow rolling on ICAM-1 is mediated by high-affinity LFA-1.

DISCUSSION

The shear flow assay mimics a cascade of adhesion reactions that cause a leukocyte in blood to engage with the vasculature following normal recirculation or inflammation. Triggering of selectin and integrin receptors sequentially causes fast and slow rolling, firm adhesion, and then migration of leukocytes into tissues. The Leukotrack program provides, for the first time that we are aware of, a fully automated procedure for quantifying the diverse behaviors of leukocytes as they bind to the different adhesion receptors that are vital for their extravasation into tissues. Desirable features of the program are its efficiency in terms of the experimenter's time and the fact that it can be used to assess various attaching cell behaviors without prior bias. Cell images are obtained using phase contrast microscopy and image analysis is performed in two steps. First, individual cells are identified in each frame of the video sequence and, in a second step, the trajectories of each cell are calculated on the basis of spatial proximity of cells in time. We can track the behavior of every cell in the assay with no limitation on numbers of analyzed cells. For example, the analysis of ~200 cells occupies ~45 min computational time per average 10-min assay. Furthermore, data can be input in batches, allowing consecutive analysis of multiple assays. This contrasts with both the 30–50 cells that are usually under observation and the time-consuming manual counting required to evaluate a single assay.

We have used the Leukotrack program to examine the role of kindlin-3 in the LFA-1-mediated behavior of B cells as they contact purified ligands ICAM-1 and E-selectin under shear flow conditions. LAD-III B cells that lack kindlin-3 are unable to roll slowly on or attach firmly to ICAM-1, events that we have shown in a previous study to require LFA-1 (48). Kindlin-3 is therefore essential for the first stage of LFA-1 attaching via ICAM-1 that follows on from fast rolling on selectins. Similarly, Alon and colleagues (49) have demonstrated an inability of LAD-III T and B lymphocytes to form the transient adhesions that support slow rolling.

In addition, we also have shown that slow rolling has a dependency on talin as determined by siRNA silencing and by use of peptides that block the talin binding site on the $\beta 2$ cytoplasmic tail, in keeping with other reports (44,46). In contrast, a recent analysis of E-selectin-stimulated slow rolling of neutrophils on purified ICAM-1 described a distinct requirement only for talin, but none for kindlin-3 (46). In our assay, the end result of E-selectin signaling was firm adhesion of B cells to ICAM-1, contrasting with the study of Lefort et al. (46) in which only neutrophil slow rolling was observed. E-selectin signaling seems therefore to have a different outcome in neutrophils compared with lymphocytes in terms of LFA-1 activation. It is worth noting that shear assays of neutrophils rolling

on E-selectin/ICAM-1-expressing L cells did result in firm adhesion (7).

An explanation for the differences between this study and that of Lefort and colleagues (46) might be that *Fermt3*$^{-/-}$ mice can compensate for lack of kindlin-3. Moreover, their method of measuring slow rolling might differ from the methodology that we report here. Lefort et al. carried out their assays at a shear flow rate of 6 dyn cm^{-2}. Our assays were chiefly conducted at a shear flow rate of 2 dyn cm^{-2}, but raising the rate to 6 dyn cm^{-2} did not alter the findings (data not shown). Thus, at present, the basis for this distinction between neutrophil and lymphocyte in the use of kindlin-3 for the more transient LFA-1 attachments involved in slow rolling remains unexplained.

It is well established that LFA-1-mediated firm adhesion of lymphocytes and neutrophils is mediated by high-affinity LFA-1 and requires both talin and kindlin-3 (9,10,26). However, a question is whether B cell slow rolling relies on an intermediate affinity form of LFA-1 to deliver the more transient adhesion. However, this is not the situation as the need for high-affinity LFA-1 was confirmed by the negative effect on slow rolling of α/β antagonist compound XVA143 that blocks formation of high-affinity LFA-1 (31). Our demonstration that E-selectin signaling results in an LFA-1 conformation that binds mAb 24, which recognizes an epitope exposed on the high-affinity form (15,38,50), provides further evidence that high-affinity LFA-1 is necessary for slow rolling as well as firm adhesion of B cells under shear flow conditions.

The nature of the initial B cell LFA-1 that binds ICAM-1 giving rise to this active integrin state is not certain. A small population of preexisting high-affinity LFA-1 with open headpiece exists on primed lymphocytes as part of the equilibrium between closed inactive and open active LFA-1. This mix of binding abilities may represent intermediate affinity LFA-1 (15). Alternatively, the ligand-binding α subunit I domain has a closed conformation as well as several intermediate forms that might participate in the initial ICAM-1 binding that leads to LFA-1 in its high-affinity state following the effect of shear (14). In favor of a distinct intermediate affinity LFA-1 conformation is the evidence for a talin-dependent extended form of LFA-1 (44,51) that has no requirement for kindlin-3 (46). As well as the lack of E-selectin-induced KIM127 epitope on LAD-III cells that we report in this study, Alon and colleagues (49) report expression of the epitope to be deficient on LAD-III T cells. Thus, lymphocytes appear to need kindlin-3 to generate the extended form of LFA-1.

Whether kindlin-3 acts cooperatively with talin in slow rolling and whether this support is direct or indirect have also not been clear. As an indirect effect, kindlins can enhance talin function by complexing with the filamin-binding protein, migfilin, which has the capacity to uncouple filamin from the binding site shared with talin (27,52). However, our study shows that siRNA knockdown of filamin A and B (53) or, alternatively, use of a migfilin peptide that interferes with filamin binding (28,29) had no impact on LFA-1-mediated slow rolling.

It has been proposed that kindlin binding to its membrane distil NPKF binding site might assist binding of talin to its more membrane proximal NPLF binding site by altering the conformation of the β subunit tail and favorably exposing the talin site (19,23–25). The use of β2 subunit tail peptides that were both unmodified and modified in both talin and kindlin-3 binding sites provides evidence for direct binding of both these proteins at the level of the integrin in the shear flow assay. This approach does not reveal whether both proteins bind to the same β2 subunit. However, kindlin-2 and talin bind independently and not cooperatively to the β3 subunit (54,55). Another option is that kindlins together with talin promote *cis* or *trans* interactions that might lead to integrin multimerization or serve as scaffolds for other participating molecules (24,26).

Thus, our evidence, both positive and negative, indicates that the LAD-III protein kindlin-3 is essential for all LFA-1-mediated adhesions under shear flow conditions, at least for lymphocytes. Acting together with talin, kindlin-3 induces formation of high-affinity LFA-1 that in turn controls lymphocyte slow rolling and firm adhesion.

SUPPORTING MATERIAL

Two figures and one movie are available at http://www.biophysj.org/biophysj/supplemental/S0006-3495(13)00844-8.

The authors are extremely grateful to colleagues Dhira Joshi and Nicola O'Reilly (Protein and Peptide Chemistry, Cancer Research UK, London Research Institute, London, UK) for peptide synthesis, Paul Gillespie (Roche, Nutley, NJ) for a supply of compound XVA143, and Dave Calderwood (Yale School of Medicine) for filamin B Ab.

The project was funded by Cancer Research UK. F.W. is supported by a Wellcome Trust Career Re-Entry Fellowship.

REFERENCES

1. Nourshargh, S., P. L. Hordijk, and M. Sixt. 2010. Breaching multiple barriers: leukocyte motility through venular walls and the interstitium. *Nat. Rev. Mol. Cell Biol.* 11:366–378.
2. Chaffer, C. L., and R. A. Weinberg. 2011. A perspective on cancer cell metastasis. *Science.* 331:1559–1564.
3. Mazo, I. B., S. Massberg, and U. H. von Andrian. 2011. Hematopoietic stem and progenitor cell trafficking. *Trends Immunol.* 32:493–503.
4. Thomas, W., M. Forero, …, V. Vogel. 2006. Catch-bond model derived from allostery explains force-activated bacterial adhesion. *Biophys. J.* 90:753–764.
5. Kim, M. J., and K. Rhee. 2011. Computational analysis of nanoparticle adhesion to endothelium: effects of kinetic rate constants and wall shear rates. *Med. Biol. Eng. Comput.* 49:733–741.
6. Lawrence, M. B., and T. A. Springer. 1991. Leukocytes roll on a selectin at physiologic flow rates: distinction from and prerequisite for adhesion through integrins. *Cell.* 65:859–873.
7. Simon, S. I., Y. Hu, …, C. W. Smith. 2000. Neutrophil tethering on E-selectin activates beta 2 integrin binding to ICAM-1 through a

mitogen-activated protein kinase signal transduction pathway. *J. Immunol.* 164:4348–4358.

8. McEver, R. P., and C. Zhu. 2010. Rolling cell adhesion. *Annu. Rev. Cell Dev. Biol.* 26:363–396.
9. Hogg, N., I. Patzak, and F. Willenbrock. 2011. The insider's guide to leukocyte integrin signalling and function. *Nat. Rev. Immunol.* 11:416–426.
10. Lefort, C. T., and K. Ley. 2012. Neutrophil arrest by LFA-1 activation. *Front. Immunol.* 3:157.
11. Alon, R., and S. W. Feigelson. 2012. Chemokine-triggered leukocyte arrest: force-regulated bi-directional integrin activation in quantal adhesive contacts. *Curr. Opin. Cell Biol.* 24:670–676.
12. Luo, B. H., C. V. Carman, and T. A. Springer. 2007. Structural basis of integrin regulation and signaling. *Annu. Rev. Immunol.* 25:619–647.
13. Schürpf, T., and T. A. Springer. 2011. Regulation of integrin affinity on cell surfaces. *EMBO J.* 30:4712–4727.
14. Xie, C., J. Zhu, …, T. A. Springer. 2010. Structure of an integrin with an alphaI domain, complement receptor type 4. *EMBO J.* 29:666–679.
15. Chen, X., C. Xie, …, T. A. Springer. 2010. Requirement of open headpiece conformation for activation of leukocyte integrin alphaXbeta2. *Proc. Natl. Acad. Sci. USA.* 107:14727–14732.
16. Woolf, E., I. Grigorova, …, R. Alon. 2007. Lymph node chemokines promote sustained T lymphocyte motility without triggering stable integrin adhesiveness in the absence of shear forces. *Nat. Immunol.* 8:1076–1085.
17. Alon, R., and M. L. Dustin. 2007. Force as a facilitator of integrin conformational changes during leukocyte arrest on blood vessels and antigen-presenting cells. *Immunity.* 26:17–27.
18. Chen, W., J. Lou, and C. Zhu. 2010. Forcing switch from short- to intermediate- and long-lived states of the alphaA domain generates LFA-1/ICAM-1 catch bonds. *J. Biol. Chem.* 285:35967–35978.
19. Malinin, N. L., E. F. Plow, and T. V. Byzova. 2010. Kindlins in FERM adhesion. *Blood.* 115:4011–4017.
20. van de Vijver, E., A. Maddalena, …, D. Roos. 2012. Hematologically important mutations: leukocyte adhesion deficiency (first update). *Blood Cells Mol. Dis.* 48:53–61.
21. Svensson, L., K. Howarth, …, N. Hogg. 2009. Leukocyte adhesion deficiency-III is caused by mutations in KINDLIN3 affecting integrin activation. *Nat. Med.* 15:306–312.
22. Malinin, N. L., L. Zhang, …, T. V. Byzova. 2009. A point mutation in KINDLIN3 ablates activation of three integrin subfamilies in humans. *Nat. Med.* 15:313–318.
23. Moser, M., M. Bauer, …, R. Fässler. 2009. Kindlin-3 is required for beta2 integrin-mediated leukocyte adhesion to endothelial cells. *Nat. Med.* 15:300–305.
24. Ye, F., and B. G. Petrich. 2011. Kindlin: helper, co-activator, or booster of talin in integrin activation? *Curr. Opin. Hematol.* 18:356–360.
25. Larjava, H., E. F. Plow, and C. Wu. 2008. Kindlins: essential regulators of integrin signalling and cell-matrix adhesion. *EMBO Rep.* 9:1203–1208.
26. Moser, M., K. R. Legate, …, R. Fässler. 2009. The tail of integrins, talin, and kindlins. *Science.* 324:895–899.
27. Wu, C. 2005. Migfilin and its binding partners: from cell biology to human diseases. *J. Cell Sci.* 118:659–664.
28. Lad, Y., P. Jiang, …, D. A. Calderwood. 2008. Structural basis of the migfilin–filamin interaction and competition with integrin beta tails. *J. Biol. Chem.* 283:35154–35163.
29. Ithychanda, S. S., M. Das, …, J. Qin. 2009. Migfilin, a molecular switch in regulation of integrin activation. *J. Biol. Chem.* 284:4713–4722.
30. Chase, S. D., J. L. Magnani, and S. I. Simon. 2012. E-selectin ligands as mechanosensitive receptors on neutrophils in health and disease. *Ann. Biomed. Eng.* 40:849–859.
31. Shimaoka, M., A. Salas, …, T. A. Springer. 2003. Small molecule integrin antagonists that bind to the beta2 subunit I-like domain and activate signals in one direction and block them in the other. *Immunity.* 19:391–402.
32. Yang, W., C. V. Carman, …, T. A. Springer. 2006. A small molecule agonist of an integrin, alphaLbeta2. *J. Biol. Chem.* 281:37904–37912.
33. Nagahara, H., A. M. Vocero-Akbani, …, S. F. Dowdy. 1998. Transduction of full-length TAT fusion proteins into mammalian cells: TAT-p27Kip1 induces cell migration. *Nat. Med.* 4:1449–1452.
34. Derossi, D., G. Chassaing, and A. Prochiantz. 1998. Trojan peptides: the penetratin system for intracellular delivery. *Trends Cell Biol.* 8:84–87.
35. Evans, R., A. C. Lellouch, …, N. Hogg. 2011. The integrin LFA-1 signals through ZAP-70 to regulate expression of high-affinity LFA-1 on T lymphocytes. *Blood.* 117:3331–3342.
36. Huang, C., Q. Zang, …, T. A. Springer. 2000. Structural and functional studies with antibodies to the integrin beta 2 subunit. A model for the I-like domain. *J. Biol. Chem.* 275:21514–21524.
37. Beglova, N., S. C. Blacklow, …, T. A. Springer. 2002. Cysteine-rich module structure reveals a fulcrum for integrin rearrangement upon activation. *Nat. Struct. Biol.* 9:282–287.
38. Dransfield, I., and N. Hogg. 1989. Regulated expression of Mg2+ binding epitope on leukocyte integrin alpha subunits. *EMBO J.* 8:3759–3765.
39. Green, C. E., U. Y. Schaff, …, S. I. Simon. 2006. Dynamic shifts in LFA-1 affinity regulate neutrophil rolling, arrest, and transmigration on inflamed endothelium. *Blood.* 107:2101–2111.
40. Koenderink, J. J. 1984. The structure of images. *Biol. Cybern.* 50:363–370.
41. Zarbock, A., C. A. Lowell, and K. Ley. 2007. Spleen tyrosine kinase Syk is necessary for E-selectin-induced alpha(L)beta(2) integrin-mediated rolling on intercellular adhesion molecule-1. *Immunity.* 26:773–783.
42. Yago, T., B. Shao, …, R. P. McEver. 2010. E-selectin engages PSGL-1 and CD44 through a common signaling pathway to induce integrin alphaLbeta2-mediated slow leukocyte rolling. *Blood.* 116:485–494.
43. Salas, A., M. Shimaoka, …, T. A. Springer. 2004. Rolling adhesion through an extended conformation of integrin alphaLbeta2 and relation to alpha I and beta I-like domain interaction. *Immunity.* 20:393–406.
44. Ebisuno, Y., K. Katagiri, …, T. Kinashi. 2010. Rap1 controls lymphocyte adhesion cascade and interstitial migration within lymph nodes in RAPL-dependent and -independent manners. *Blood.* 115:804–814.
45. Kuwano, Y., O. Spelten, …, A. Zarbock. 2010. Rolling on E- or P-selectin induces the extended but not high-affinity conformation of LFA-1 in neutrophils. *Blood.* 116:617–624.
46. Lefort, C. T., J. Rossaint, …, K. Ley. 2012. Distinct roles for talin-1 and kindlin-3 in LFA-1 extension and affinity regulation. *Blood.* 119:4275–4282.
47. Kim, M., C. V. Carman, and T. A. Springer. 2003. Bidirectional transmembrane signaling by cytoplasmic domain separation in integrins. *Science.* 301:1720–1725.
48. Henderson, R. B., L. H. Lim, …, N. Hogg. 2001. The use of lymphocyte function-associated antigen (LFA)-1-deficient mice to determine the role of LFA-1, Mac-1, and alpha4 integrin in the inflammatory response of neutrophils. *J. Exp. Med.* 194:219–226.
49. Manevich-Mendelson, E., S. W. Feigelson, …, R. Alon. 2009. Loss of kindlin-3 in LAD-III eliminates LFA-1 but not VLA-4 adhesiveness developed under shear flow conditions. *Blood.* 114:2344–2353.
50. Kamata, T., K. K. Tieu, …, Y. Takada. 2002. The role of the CPNKEKEC sequence in the beta(2) subunit I domain in regulation of integrin alpha(L)beta(2) (LFA-1). *J. Immunol.* 168:2296–2301.
51. Li, Y. F., R. H. Tang, …, S. M. Tan. 2007. The cytosolic protein talin induces an intermediate affinity integrin alphaLbeta2. *J. Biol. Chem.* 282:24310–24319.
52. Kiema, T., Y. Lad, …, D. A. Calderwood. 2006. The molecular basis of filamin binding to integrins and competition with talin. *Mol. Cell.* 21:337–347.

53. Baldassarre, M., Z. Razinia, …, D. A. Calderwood. 2009. Filamins regulate cell spreading and initiation of cell migration. *PLoS ONE.* 4:e7830.

54. Kahner, B. N., H. Kato, …, F. Ye. 2012. Kindlins, integrin activation and the regulation of talin recruitment to αIIbβ3. *PLoS ONE.* 7:e34056.

55. Bledzka, K., J. Liu, …, E. F. Plow. 2012. Spatial coordination of kindlin-2 with talin head domain in interaction with integrin β cytoplasmic tails. *J. Biol. Chem.* 287:24585–24594.

56. Constantin, G., M. Majeed, …, C. Laudanna. 2000. Chemokines trigger immediate beta2 integrin affinity and mobility changes: differential regulation and roles in lymphocyte arrest under flow. *Immunity.* 13:759–769.

57. García-Bernal, D., M. Parmo-Cabañas, …, J. Teixidó. 2009. Chemokine-induced Zap70 kinase-mediated dissociation of the Vav1–talin complex activates alpha4beta1 integrin for T cell adhesion. *Immunity.* 31:953–964.

58. Smith, D. F., T. L. Deem, …, K. Ley. 2006. Leukocyte phosphoinositide-3 kinase gamma is required for chemokine-induced, sustained adhesion under flow in vivo. *J. Leukoc. Biol.* 80:1491–1499.

59. Zarbock, A., C. L. Abram, …, K. Ley. 2008. PSGL-1 engagement by E-selectin signals through Src kinase Fgr and ITAM adapters DAP12 and FcR gamma to induce slow leukocyte rolling. *J. Exp. Med.* 205:2339–2347.